PAPER

Check for updates

Elemental doping inhibits surface-state-mediated charge carrier trapping for promoting photocatalytic selective oxidation†

Yan Zhao,‡[a] Wenxiu Liu,‡[a] Wei Shao,‡[a] Lei Li,[a] Ming Zuo,[a] Jun Hu,[c] Junfa Zhu, [ID][c] Hui Wang*[ab] and Xiaodong Zhang [ID] *[ab]

The surface-state-mediated trapping process, a dominant consumption pathway of photoinduced charge carriers, sometimes plays a detrimental role in gaining high-efficiency photocatalytic solar energy utilization. Herein, taking $Bi_2O_2CO_3$ as a typical prototype, we highlight that vanadium doping could effectively inhibit surface-state-mediated charge carrier trapping in the system. According to spectral analyses and theoretical calculations, we attributed such an inhibition to the presence of shallow trap states close to band edges induced by vanadium doping. Compared with surface states, these vanadium-doping-induced states could trap photoinduced charge carriers, whereas their shallow feature facilitates charge carrier de-trapping. Benefiting from these characteristics, vanadium-doped $Bi_2O_2CO_3$ (V–$Bi_2O_2CO_3$) exhibits promoted performance in photocatalytic molecular oxygen activation and selective aerobic oxidation of organic compounds. This work provides an effective method for suppressing the detrimental charge-carrier-trapping mediated by surface states in semiconductor-based photocatalysis.

Introduction

Ever since its first report in 1972, semiconductor-based photocatalysis has been attracting tremendous attention by virtue of its prominent advantage in converting solar energy to chemical energy that would facilitate the solving of energy and environmental issues.[1–5] As a precondition for gaining high-efficiency photocatalytic energy conversion, the separation and transfer of photoinduced charge carriers in semiconductor-based photocatalysts are crucial, and the corresponding regulations are always the research highlights. However, owing to the widespread imperfections (like dopants, vacancies, interfaces, *etc.*) in semiconductor crystals, there are various nonradiative or radiative decay pathways that would lead to unfavorable consumption of charge carriers, which has a detrimental effect on the relevant photocatalytic energy utilization.[6–9] Among these imperfections, a surface with chemical-bond breaking and active-atom exposure usually gives rise to abundant states

that would lead to the trapping of photoinduced charge carriers.[10–13] Thus, understanding the impacts of surface-state-mediated charge carrier trapping on photocatalysis and exploring effective strategies to eliminate the negative effects are necessary.

Surface-state-mediated charge carrier trapping would play a detrimental role in photocatalysis when these states exhibit deep-lying energy-level features. In detail, when charge carriers are trapped by surface states with deep-lying energy levels, their redox capacities would be limited compared with those of band-edge positions. Besides, the large variation between energy levels of deep-lying surface states and band-edge states (including the conduction band minimum and valence band maximum) set restrictions on carrier de-trapping. The above effects inhibit the separation and transfer of charge carriers and hence their participations in photocatalysis.[14,15] Considering that there are various trapping processes and recombination centers whose competitions jointly determine charge carrier behaviors, we deduce that constructing shallow trapping states might be feasible to inhibit the detrimental effects of surface-state-mediated charge carrier trapping. On the one hand, shallow trapping states would provide an additional pathway for accommodating photoinduced charge carriers; on the other hand, charge carriers trapped by shallow states hold appropriate redox capacities and de-trapping probabilities.

Compared with trapping states caused by other imperfections, surface trapping states are notably dependent on the crystal orientation and exotic environment. That is, surface

[a]Hefei National Research Center for Physical Sciences at the Microscale, University of Science and Technology of China, Hefei, Anhui 230026, P. R. China. E-mail: wanghuig@ustc.edu.cn; zhxid@ustc.edu.cn

[b]Institute of Energy, Hefei Comprehensive National Science Center, Hefei, Anhui 230031, P. R. China

[c]National Synchrotron Radiation Laboratory, University of Science and Technology of China, Hefei, Anhui 230029, China

† Electronic supplementary information (ESI) available. See DOI: https://doi.org/10.1039/d2ta09702h

‡ These authors contributed equally to this work.
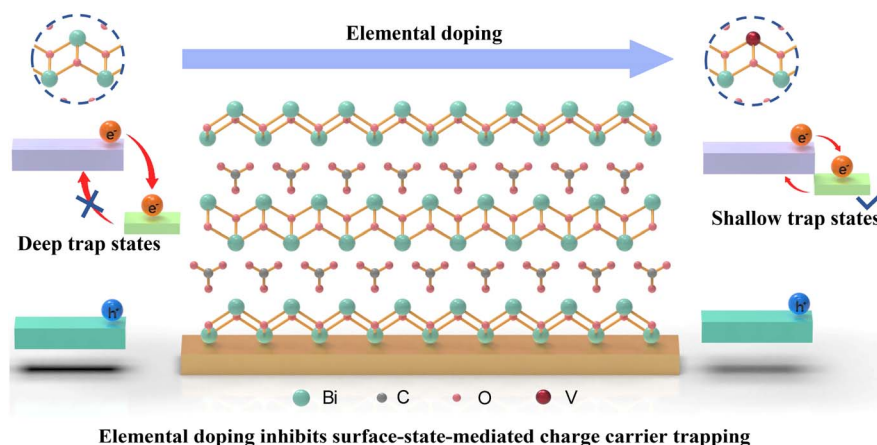
Scheme 1 Scheme of the V doping inhibited surface state mediated charge carrier trapping of V-$Bi_2O_2CO_3$.

atomic exposure and exotic atom adsorption would greatly impact their energy levels and hence the behaviors of trapping charge carriers, which undoubtedly complicate the relevant investigations. In this case, searching for suitable systems with definite surface structures would be favorable. Herein, we focus our attention on $Bi_2O_2CO_3$, whose anisotropic hetero-layered structure enables an ideal prototype for investigating the role of surface trapping states in photocatalysis (Scheme 1). As a typical transition metal, V doping in inorganic compounds typically induces V-3d states below the conduction band minimum, contributing to the transfer of photoexcited electrons to the conduction band.[16] In addition, the V element has variable valence and the charge migration helps to trap photoexcited carriers (electrons and holes), thus reducing the complexation rate.[17] We demonstrate that surface-state-mediated charge carrier trapping was significantly suppressed by a trace-vanadium-doping treatment. According to density
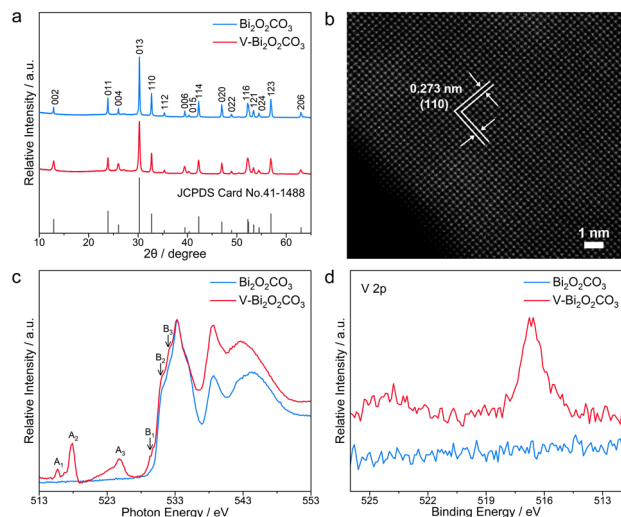
functional theory (DFT) calculations (Fig. 1c–f), the conduction band charge of pristine $Bi_2O_2CO_3$ is mainly distributed in the $[Bi_2O_2]^{2+}$ layer, whereas notable contributions from vanadium atoms could be found in the doped system. In addition, density of states (DOS) at the bottom of the conduction band increases in the doped sample (Fig. 1a and b), indicating the formation of a shallow trap state. Therefore, it would be anticipated that vanadium-doped $Bi_2O_2CO_3$ (V-$Bi_2O_2CO_3$) exhibits promoted photocatalytic performance in reactions like molecular oxygen activation and selective aerobic oxidation.

Results and discussion

In this study, vanadium-doped $Bi_2O_2CO_3$ (denoted as V-$Bi_2O_2CO_3$) and pristine $Bi_2O_2CO_3$ were synthesized by a modified hydrothermal method (see details in the ESI†). The structure of the as-prepared samples was studied by X-ray diffraction (XRD) measurements (Fig. 2a and S1†), where the doped sample shows a nearly identical pattern compared with that of pristine $Bi_2O_2CO_3$, indicating the maintained matrix structure. Electron microscopy techniques were employed to investigate detailed morphological and structural information. As shown in Fig. S2 and S3,† the scanning electron microscopy (SEM) and transmission electron microscopy (TEM) images suggest that both pristine $Bi_2O_2CO_3$ and V-$Bi_2O_2CO_3$ show a plate-like morphology with a lateral width of ~1 μm. The high-angle annular dark-field scanning transmission electron microscopy (HAADF-STEM) image in Fig. 2b displays obvious lattice fringes with a spacing of 0.273 nm, indexed to the (110) planes of V-$Bi_2O_2CO_3$ which is consistent with that of pristine $Bi_2O_2CO_3$ (Fig. S4†). The subsequent element mapping results present the homogeneous distributions of V, O, C, and Bi all over the whole sample, as shown in Fig. S5.† In view of its notable advantages in characterizing elemental and coordination environments, X-ray absorption near edge structure (XANES) measurement was carried out, where Fig. 2c displays the V $L_{2,3}$ and O K-edge XANES spectra. Notably, compared with that of $Bi_2O_2CO_3$, XANES spectra of V-$Bi_2O_2CO_3$ exhibit six new peaks labeled A_1, A_2, A_3, B_1, B_2, and B_3. The first three peaks (*i.e.*, A_1, A_2, and A_3)
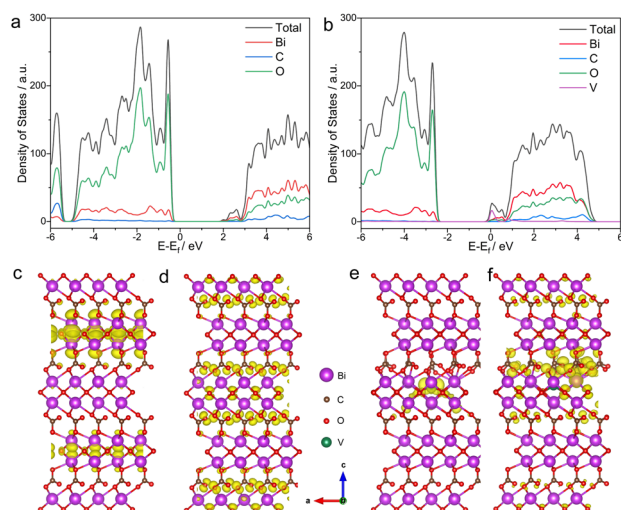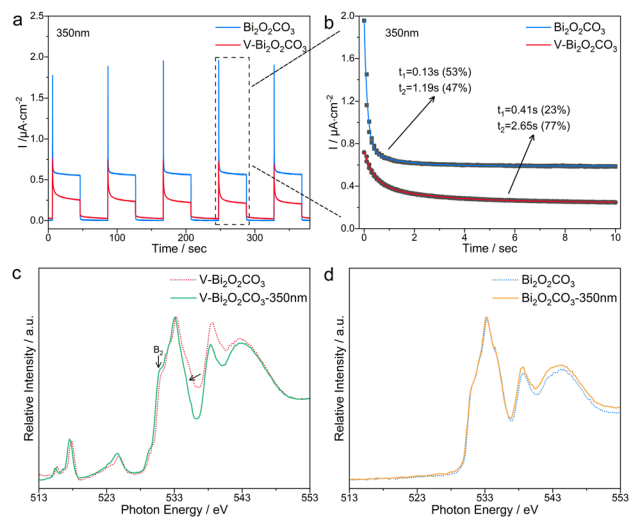

Fig. 1 Calculated DOS of (a) $Bi_2O_2CO_3$ and (b) V-$Bi_2O_2CO_3$; charge density isosurfaces of $Bi_2O_2CO_3$ (c) conduction band and (d) valence band; charge density isosurfaces of vanadium-doped $Bi_2O_2CO_3$ (e) conduction band and (f) valence band.

This journal is © The Royal Society of Chemistry 2023

J. Mater. Chem. A, 2023, **11**, 3594–3598 | **3595**

Fig. 2 (a) XRD patterns of V-Bi$_2$O$_2$CO$_3$ and Bi$_2$O$_2$CO$_3$, respectively; (b) atomic-resolution HAADF-STEM image of V-Bi$_2$O$_2$CO$_3$; (c) XANES spectra of V-Bi$_2$O$_2$CO$_3$ and Bi$_2$O$_2$CO$_3$ at V L$_{2,3}$ and O K edge regions; (d) V 2p XPS spectra of Bi$_2$O$_2$CO$_3$ and V-Bi$_2$O$_2$CO$_3$.

Fig. 3 (a) Transient photocurrent responses at 0.6 V; (b) photocurrent decay curves extracted from (panel a), and the corresponding fitting results; XANES spectra of (c) V-Bi$_2$O$_2$CO$_3$ and (d) Bi$_2$O$_2$CO$_3$ at the V L$_{2,3}$ and O K edge regions with/without 350 nm illumination.

peaking at ~515.7, 517.8, and 524.8 eV correspond to the V L$_{2,3}$ edge region. In detail, peak A$_1$ would be related to the electronic transition from V 2p to unoccupied V 4s states, indicating that V atoms do not exist in metallic form. Meanwhile, peak A$_2$ and A$_3$ would be assigned to the transitions of electrons from 2p$_{3/2}$ and 2p$_{1/2}$ energy levels to the V 3d–O 2p hybridization band. Besides, the O K-edge region shows three peaks B$_1$, B$_2$, and B$_3$ at about 529.4, 531.0, and 532.2 eV that could be ascribed to transitions from O 1s to the V 3d–O 2p hybridization band.[18,19] The XANES results clearly demonstrate the successful doping of V elements and the formation of V–O bonds. X-ray photoelectron spectroscopy (XPS) measurement was performed to investigate the elemental components and chemical states of V-Bi$_2$O$_2$CO$_3$ and Bi$_2$O$_2$CO$_3$ (Fig. 2d and S6†), where an obvious V signal could be observed for V-Bi$_2$O$_2$CO$_3$. Moreover, the Raman spectra (Fig. S7†) confirm that the vibration related to the [Bi$_2$O$_2$]$^{2+}$ layer (352 cm^{-1})[20] exhibits about a 4 cm^{-1} red shift in V-Bi$_2$O$_2$CO$_3$, suggesting that vanadium doping would effectively modify Bi–O vibration scenarios. The above results confirm successful vanadium doping in the Bi$_2$O$_2$CO$_3$ system.

Vanadium doping is anticipated to impact the relaxation of photoinduced charge carriers in Bi$_2$O$_2$CO$_3$, which was studied by electrochemical analyses. As shown in Fig. 3a, Bi$_2$O$_2$CO$_3$ exhibits a very high initial photocurrent spike and decays to the steady state faster than V-Bi$_2$O$_2$CO$_3$ under 350 nm illumination at a 0.6 V bias voltage. It is found that the fitted relaxation times of photocurrent for Bi$_2$O$_2$CO$_3$ and V-Bi$_2$O$_2$CO$_3$ were ~0.14 and 0.41 s, respectively. These results clearly prove the suppressed consumption of photoinduced charge carriers in V-Bi$_2$O$_2$CO$_3$.[21–24] Besides, the potential impacts of electrical conductivity on the photocurrent spike were excluded by electrochemical impedance spectroscopy (EIS) measurements (Fig. S8†). To verify the origin of the photocurrent spike, atmosphere-dependent photocurrent response measurements were

conducted. Fig. S9† displays photocurrent responses under O$_2$, N$_2$, and air atmospheres, where strikingly different atmosphere dependences could be observed for Bi$_2$O$_2$CO$_3$ and V-Bi$_2$O$_2$CO$_3$ cases. In detail, the intensity of photocurrent at the stable stage of Bi$_2$O$_2$CO$_3$ increases with the O$_2$ concentration, while that of V-Bi$_2$O$_2$CO$_3$ exhibits negligible dependence on the atmosphere. These features could be understood as follows: increased O$_2$ concentration leads to promoted adsorption of oxygen molecules on the surface, which would passivate the surface trapping state to some extent. Negligible variations in photocurrent responses of V-Bi$_2$O$_2$CO$_3$ under different atmospheres suggest that vanadium doping could passivate surface-state-mediated charge carrier trapping. The above deduction could be further evidenced by photoluminescence (PL) measurements (Fig. S10†), where obvious reduction in PL emission intensity could be observed for the V-Bi$_2$O$_2$CO$_3$ sample. As for the fact that V-Bi$_2$O$_2$CO$_3$ possesses a lower stable-stage than Bi$_2$O$_2$CO$_3$, this may related to the modified band structure in V-Bi$_2$O$_2$CO$_3$ (as evidenced by UV-vis and valence band spectra in Fig. S11†), leading to an unexpected energy level mismatch with respect to ITO glass.[25–27] To go further, XANES measurements under light and dark conditions were carried out to gain insights into the mechanism of suppressing charge carrier trapping by vanadium doping. As displayed in Fig. 3c, a narrowed 535.0 eV peak and an increased peak B$_2$ under light conditions could be found for V-Bi$_2$O$_2$CO$_3$. The above changes in the XANES spectra suggest the decreased electron-occupying state of O atoms under light illumination, and electrons are most likely to be trapped by vanadium-dopant-related states. By contrast, no obvious changes in XANES characteristics could be found for the Bi$_2$O$_2$CO$_3$ case (Fig. 3d).

In view of its suppressed surface-state-mediated charge carrier trapping, V-Bi$_2$O$_2$CO$_3$ is anticipated to hold promoted photocatalytic performance. By virtue of its significance in fields
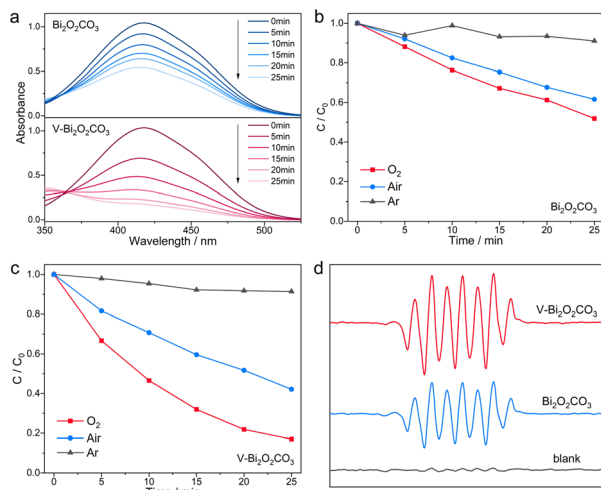
Fig. 4 Photocatalytic molecular oxygen activation. (a) Time-dependent absorption spectra of MO oxidation with different catalysts under an oxygen atmosphere; (b and c) evolutions of the absorbance peak monitored for the product at 417 nm under different gas conditions; (d) ESR-trapping tests of different samples in the presence of DMPO.

such as pollutant treatment and organic synthesis, photocatalytic molecular oxygen activation was carried out to evaluate the performance of both the samples, using methyl orange (MO) as a probe molecule. As exhibited in Fig. 4a, V-$Bi_2O_2CO_3$ exhibits a higher MO degradation rate than pristine $Bi_2O_2CO_3$ under full-spectrum light. The degradation of MO was found to be related to photocatalytic molecular oxygen activation, as demonstrated by the positive correlation between the MO degradation rate and oxygen concentration for both samples (Fig. 4b and c). According to previous reports,[28] H_2O_2 was verified as the dominant reactive species produced by $Bi_2O_2CO_3$. Here, ESR-trapping tests were carried out by taking 5,5-dimethyl-1-pyrroline-N-oxide (DMPO) as the trapping agent. As shown in Fig. 4d, the generated peak represents the oxidation of DMPO by H_2O_2, and V-$Bi_2O_2CO_3$ has stronger H_2O_2 generation capacity. The above results confirm the promoted photocatalytic performance of V-$Bi_2O_2CO_3$ in molecular oxygen activation, which corresponds with the involved suppressed surface-state-mediated charge carrier trapping.

The promoted photocatalytic molecular oxygen activation of V-$Bi_2O_2CO_3$ promises its application in selective oxidation reactions. Here, we investigate its potential in photocatalytic oxidative coupling of benzylamines. As shown in Table 1, V-$Bi_2O_2CO_3$ under oxygen exhibits significantly higher catalytic properties in converting benzylamine to the corresponding imine than pristine $Bi_2O_2CO_3$ (entry 1). Furthermore, the suppression of benzylamine coupling under argon conditions (entry 2) proves that oxygen is required for triggering the reaction. The catalytic performance of V-$Bi_2O_2CO_3$ decreased significantly when isopropyl alcohol (hole scavenger) was added confirming that the oxidative coupling of benzylamine was relative to photoinduced holes. Furthermore, the scope of oxidative coupling of benzylamines triggered by V-$Bi_2O_2CO_3$ was investigated, where a series of benzylamine derivatives was

Table 1 Oxidative coupling of benzylamine[a]

● C ● H ● N ● P-substitution ● M-substitution ● O-substitution

| Entry | R | t/h | $Bi_2O_2CO_3$ | | V-$Bi_2O_2CO_3$ | |
			Conv.[b]	Select.[c]	Conv.[b]	Select.[c]
1	H	5	37	99	99	99
2[d]	H	5	Trace	Trace	Trace	Trace
3[e]	H	5	33	99	43	99
4	O-Me	6	41	82	99	99
5	m-Me	8	31	84	92	92
6	p-Me	8	33	85	78	95
7	p-F	8	45	99	76	94
8	p-Cl	8	41	99	82	94
9	p-Br	6	53	99	99	99

[a] Reaction conditions: catalyst (5 mg), benzylamine (20 μL), acetonitrile (2 mL), xenon lamp (300 W), 298 K, O_2 (1 atm). [b] Determined by ^{1}H NMR spectroscopy using 1,1,2,2-tetrachloroethane as the internal standard substance, mol%. [c] Selectivity = yield/conversion, mol%. [d] Ar, 1 atm. [e] Additional isopropyl alcohol (200 μL).

selected. It could be seen that V-$Bi_2O_2CO_3$ exhibited promoted conversion efficiency in converting benzylamine derivatives with different-type and -position substituents into the corresponding imines, compared with pristine $Bi_2O_2CO_3$, which was in accordance with the positive role of vanadium doping in suppressing surface-state-mediated charge carrier trapping. It is noteworthy that compared with the original catalyst, the sample after reaction possesses similar XPS characteristic spectra (Fig. S12†) and maintained stable cycling performance after 5 consecutive photocatalytic cycles (Fig. S13†). From the above results, it could be concluded that V-$Bi_2O_2CO_3$ holds great potential in triggering selective oxidation reactions.

Conclusions

In summary, we exploited an effective strategy for suppressing the consumption of photoinduced charge carriers produced by surface-state-mediated trapping processes in semiconductor-based photocatalysts. Taking $Bi_2O_2CO_3$ as an example, we demonstrated that vanadium doping could strikingly suppress surface-state-mediated charge carrier trapping as demonstrated by both of the theoretical and experimental results. In detail, DFT calculations indicate that the incorporation of vanadium atoms in a $Bi_2O_2CO_3$ system could form shallow trapping states below the conduction band, which would compete with the deep-lying energy-level surface states for accommodating photoinduced charge carriers. On the basis of electrochemical and spectroscopic analyses, we confirmed the participation of vanadium dopants in photoexcitation processes of the $Bi_2O_2CO_3$ system, which plays a positive role in suppressing the

This journal is © The Royal Society of Chemistry 2023

J. Mater. Chem. A, 2023, **11**, 3594–3598 | **3597**

rapid charge carrier trapping by surface states. Benefitting from this feature, vanadium-doped $Bi_2O_2CO_3$ exhibits a predominant advantage in triggering photocatalytic reactions like molecular oxygen activation and selective aerobic oxidation. This work provides a feasible strategy for regulating charge-carrier trapping in semiconductor-based photocatalysts.

Author contributions

Y. Z., W. L. and W. S. contributed equally to this work. Y. Z. conceived the idea, performed the experiments and collected the data; L. L. conducted and analyzed the DFT calculations; M. Z. conducted the HRTEM experiments; Y. Z., W. L., and W. S. co-wrote the manuscript; X. Z. and H. W. supervised the project. All authors contributed to the overall scientific interpretation and editing of the manuscript.

Conflicts of interest

The authors declare that they have no competing interests.

Acknowledgements

References

1 A. Fujishima and K. Honda, *Nature*, 1972, **238**, 37–38.

2 A. Mills and S. LeHunte, *J. Photochem. Photobiol., A*, 1997, **108**, 1–35.

3 M. R. Hoffmann, S. T. Martin, W. Y. Choi and D. W. Bahnemann, *Chem. Rev.*, 1995, **95**, 69–96.

4 M. Wang, J. Ioccozia, L. Sun, C. Lin and Z. Lin, *Energy Environ. Sci.*, 2014, **7**, 2182–2202.

5 A. Mills, R. H. Davies and D. Worsley, *Chem. Soc. Rev.*, 1993, **22**, 417–425.

6 M. T. Mbumba, D. M. Malouangou, J. M. Tsiba, M. W. Akram, L. Bai, Y. Yang and M. Guli, *J. Mater. Chem. C*, 2021, **9**, 14047–14064.

7 A. Veamatahau, B. Jiang, T. Seifert, S. Makuta, K. Latham, M. Kanehara, T. Teranishi and Y. Tachibana, *Phys. Chem. Chem. Phys.*, 2015, **17**, 2850–2858.

8 G. Konstantatos, L. Levina, A. Fischer and E. H. Sargent, *Nano Lett.*, 2008, **8**, 1446–1450.

9 A. Stavrinadis, S. Pradhan, P. Papagiorgis, G. Itskos and G. Konstantatos, *ACS Energy Lett.*, 2017, **2**, 739–744.

10 C.-S. Tan, Y. Zhao, R. H. Guo, W. T. Chuang, L. J. Chen and M. H. Huang, *Nano Lett.*, 2020, **20**, 1952–1958.

11 H. Li, Z. Wu and M. T. Lusk, *J. Phys. Chem. C*, 2014, **118**, 46–53.

12 S. Kahmann and M. A. Loi, *Appl. Phys. Rev.*, 2020, **7**, 041305.

13 Y. Ding, M. Sugaya, Q. Liu, S. Zhou and T. Nozaki, *Nano Energy*, 2014, **10**, 322–328.

14 H. Jin, E. Debroye, M. Keshavarz, I. G. Scheblykin, M. B. J. Roeffaers, J. Hofkens and J. A. Steele, *Mater. Horiz.*, 2020, **7**, 397–410.

15 J. Jiang, C. Ling, T. Xu, W. Wang, X. Niu, A. Zafar, Z. Yan, X. Wang, Y. You, L. Sun, J. Lu, J. Wang and Z. Ni, *Adv. Mater.*, 2018, **30**, 1804322.

16 M. Khan, Y. Song, N. Chen and W. Cao, *Mater. Chem. Phys.*, 2013, **142**, 148–153.

17 H. Liu, Y. Wu and J. Zhang, *ACS Appl. Mater. Interfaces*, 2011, **3**, 1757–1764.

18 M. Faiz, N. Tabet, A. Mekki, B. S. Mun and Z. Hussain, *Thin Solid Films*, 2006, **515**, 1377–1379.

19 M. Abbate, F. M. F. Degroot, J. C. Fuggle, Y. J. Ma, C. T. Chen, F. Sette, A. Fujimori, Y. Ueda and K. Kosuge, *Phys. Rev. B: Condens. Matter Mater. Phys.*, 1991, **43**, 7263–7267.

20 W. Zhao, Y. Wang, A. Wang, J. Qian, W. Zhu, S. Dou, Q. Wang, Q. Zhong and A. Chen, *RSC Adv.*, 2017, **7**, 7658–7670.

21 H. Liu, K. Tian, J. Ning, Y. Zhong, Z. Zhang and Y. Hu, *ACS Catal.*, 2019, **9**, 1211–1219.

22 M. Mokhtarimehr and S. A. Tatarkova, *J. Opt. Soc. Am. B*, 2017, **34**, 1705–1712.

23 L. Zhang, E. Reisner and J. J. Baumberg, *Energy Environ. Sci.*, 2014, **7**, 1402–1408.

24 R. Zhang, X. Ning, Z. Wang, H. Zhao, Y. He, Z. Han, P. Du and X. Lu, *Small*, 2022, **18**, 2107938.

25 C. X. Li, B. Q. Qiu, W. L. Wang, J. L. Zhuang and J. Tang, *Thin Solid Films*, 2020, **698**, 137855.

26 J.-H. Yun, M. D. Kumar, Y. C. Park, H.-S. Kim and J. Kim, *J. Mater. Sci.: Mater. Electron.*, 2015, **26**, 6099–6106.

27 W. Dong, C. Lu, M. Luo, Y. Liu, T. Han, Y. Ge, X. Xue, Y. Zhou and X. Xu, *J. Colloid Interface Sci.*, 2022, **621**, 374–384.

28 S. Jin, H. Wang, L. Li, X. Luo, X. Sun, M. Zuo, J. Tian, X. Zhang and Y. Xie, *Sci. China: Chem.*, 2021, **64**, 1964–1969.

3598 | *J. Mater. Chem. A*, 2023, **11**, 3594–3598

This journal is © The Royal Society of Chemistry 2023